6. Density-Based Techniques

The methods dealt with in this section are based on changes of fluid density; hence its index of refraction. As a result of these changes, optical phase and, coupled with it, direction of propagation of a light wave transmitted through the flow are altered in comparison to the properties of the incident light. The available signal can be presented in planar form, i. e., as a flow picture, and the methods are often referred to as *optical flow visualisation*, because the changes in index of refraction are detected and measured by optical techniques. The obtainable information is integrated along the whole path of the light in the fluid field (*line-of-sight methods*) and, in a three-dimensional (3D) object field, special techniques for interpreting the signal pattern are necessary (*tomography*) in order to provide local data values of the quantity to be determined, e.g., density. Four major groups of experimental methods can be distinguished: shadowgraphy, schlieren technique, moiré techniques, and interferometry. The fluid mechanical problem areas to which these optical measuring techniques can be applied are compressible flow, convective heat transfer, mixing and mass transfer, combustion, and flows with density stratification.

6.1 Density, Refractive Index, and Optical Flow Visualization

The methods dealt with in this section are essentially those that provide information on the state of flow using light, which is transmitted through the flow field as depicted in Fig. 11.1 of Chap. 11. Optical phase and, coupled with it, the direction of propagation of the transmitted light wave are altered compared to the properties of the incident wave if the fluid's refractive index varies in the flow. The refractive index n is related to the fluid density through the Clausius–Mosotti equation [6.1], which for a gas reduces to the simpler form of the Gladstone–Dale equation

$$n - 1 = K\rho \qquad (6.1)$$

with ρ being the gas density and K the *Gladstone–Dale constant*, which has the dimension of $1/\rho$, is specific for a gas, and depends weakly on the wavelength of light used [6.1]. In compressible flow of an ideal gas the density ρ is a function of the Mach number [6.2], and, for these flows, the information obtainable with the methods to be discussed in this section is therefore a measure of the Mach number or flow velocity.

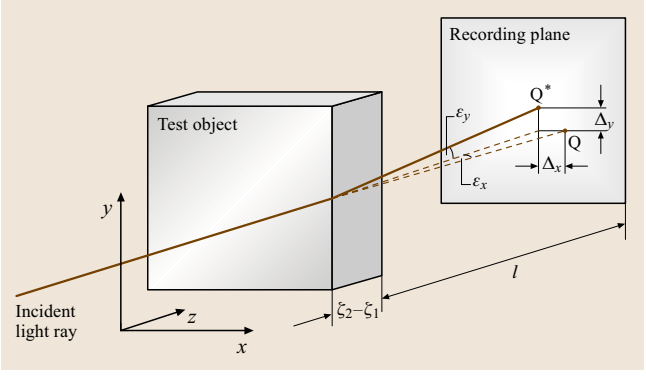

Fig. 6.1 Refractive deflection of a light ray in an object field (flow) with varying refractive index (caused by varying fluid density)

Table 6.1 Methods of optical flow visualisation

Method	Signal form	sensitive to changes of
Shadowgraph	Displacement Δ	$\partial^2\rho/\partial x^2$, $\partial^2\rho/\partial y^2$
Schlieren, moiré	Deflection angle ε	$\partial\rho/\partial x$, $\partial\rho/\partial y$
Speckle photography	Deflection angle ε	$\partial\rho/\partial x$, $\partial\rho/\partial y$
Shearing interferometry	Phase difference	$\partial\rho/\partial x$, $\partial\rho/\partial y$
Reference beam interferometry	Phase difference	ρ

The methods dealt with below collect and present the signal in planar form, i. e., as a flow picture, and they are often referred to as *optical flow visualisation*, because the aforementioned changes in optical phase are detected and measured by optical techniques. As for any *line-of-sight method* the obtainable information is integrated along the whole path of the light in the fluid field and, in a three-dimensional (3-D) object field, special techniques for desintegrating the signal pattern are necessary in order to provide local data values of the quantity to be determined, e.g., density. This desintegration, with the aim of reconstructing the 3-D object from a number of two-dimensional (2-D) data sets, requires the transmission of light waves through the object in different directions and is called optical tomography (Sect. 6.6).

The propagation of a light wave or ray through an inhomogeneous transparent object field, here a flow with variable fluid density, can be analysed by applying Fermat's principle (see [6.1] and references therein). As a result of the variation of the refractive index, the light ray is deflected from its undisturbed, original direction. The signal evidencing this deflection in a recording plane (Fig. 6.1) is either the displacement with the two components Δ_x, Δ_y or the deflection angle with its two components ε_x, ε_y; z is the direction of the incident light ray. In addition to the light deflection, the optical phase of the wave is different from the phase that the wave would have in the recording plane in the absence of the object. This difference in optical phase (or its equivalent expressed as an optical path length) can also be transformed into a visible signal. The signal patterns are collected in the recording plane, e.g., with a photographic or electronic camera. By means of the analysis of wave propagation in the refractive index field, one can relate the observable signal to the refractive index or density distribution in the flow under study.

According to the different signal forms (displacement Δ, deflection angle ε, optical phase difference) one can distinguish between three different groups of methods of optical flow visualisation. They also differ systematically in the relationship between the observable or measurable signal and the fluid density (Table 6.1).

Besides compressibility there may be other reasons for alterations of the fluid density in a flow, the most common being temperature differences as the result of heat transfer processes. Another cause is differences of concentration values in an inhomogeneous fluid with several components; the related fluid-mechanical process is mixing, which applies to both gaseous and liquid flows. Both mixing and heat transfer cause combustion processes to exhibit variations in density, so that they are often the object of optical flow visualisation. Finally, flow processes of a fluid that, in equilibrium, has a natural vertical density gradient (*stratified flow*) can be investigated with the methods discussed here. In some of these fields the techniques of optical flow visualisation were developed independently and with exclusive applicability to the respective field [6.3–5].

For a quantitative measurement of the density or one of its derivatives the exact relationship between refractive index and density must be known. Values of the Gladstone–Dale constant appearing in (6.1) or relationships applying either to pure or salted water (used for experiments with stratified flows) are included in [6.1].

6.2 Shadowgraphy

In its simplest form, the shadowgraph does not need any optical component, and the effect can therefore be observed in many situations outside of a laboratory. An essential feature of the method is the use of a point-shaped light source. The light diverging from this source is transmitted through the test object, and a shadow pattern caused by an inhomogeneous density field can be observed in a vertical plane at a distance l behind the object [6.1, 6]. More common for laboratory experiments is an arrangement with parallel light through the flow, which might be bounded by viewing windows (Fig. 6.2). In order to be able to record a shadowgraph of reduced size with a camera, the recording plane (photographic film, chip of an electronic camera) is focused by means

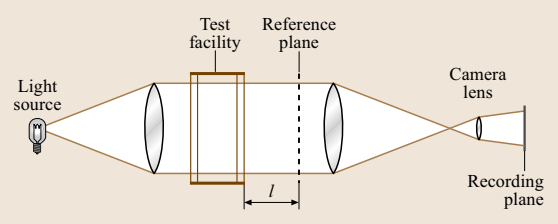

Fig. 6.2 Shadowgraph setup with parallel beams through the test object

of the camera lens onto the plane at a distance l from the object. In this way, the object is not in focus in the shadow picture.

When passing through the flow field under study, the individual light rays are refracted and bent out of their original path as indicated in Fig. 6.1, so that the light intensity in the plane of observation is altered with respect to the undisturbed case. By means of an analysis of the light propagation in the refractive index field of the object [6.1], one derives for the relative changes of light intensity in the plane of observation

$$\frac{\Delta I}{I} = l \int_{\zeta_1}^{\zeta_2} \left(\frac{\partial^2}{\partial x^2} + \frac{\partial^2}{\partial y^2} \right) (\ln n) \, \mathrm{d}z \,, \tag{6.2}$$

where I is the light intensity, l is explained in Fig. 6.2, z is the optical axis and direction of light propagation, and x and y are the coordinates in planes normal to the optical axis, $n(x, y, z)$ is the refractive index in the flow; $\Delta I/I(x, y)$ is the observable signal, i. e., a distribution of shades or values of grey in the recording plane; ζ_1 and ζ_2 are the entrance and exit coordinates, respectively, of the light rays transmitted through the test object. The integral evidences the property of all *light-of-sight* methods: The information on the quantity of interest, here density, is integrated along the light path in the object.

Equation (6.2) is derived with the assumption that the displacements of a light ray as shown in Fig. 6.1, Δ_x and Δ_y, are small, e.g., in comparison to l (*weak refraction*). By applying the Gladstone–Dale formula, (6.1), it becomes evident that the shadowgraph is sensitive to changes of the second derivative of the (gas) density. From this it follows that the shadowgraph is not a method suitable for a direct quantitative measurement of density, since such an evaluation would require one to perform a double integration of the signal data. However, owing to its simplicity, the method is convenient for obtaining a quick survey of flow fields with varying fluid density.

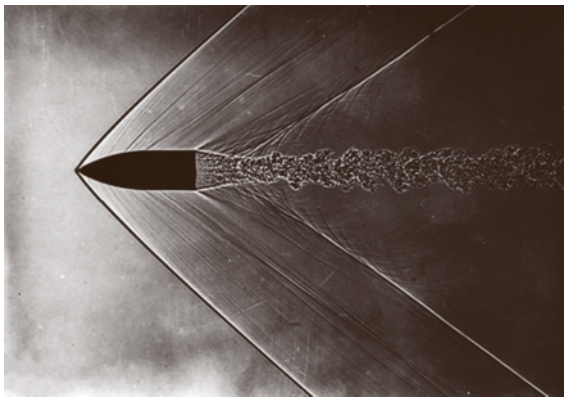

Fig. 6.3 Shadowgraph of a bullet flying at supersonic velocity (courtesy Deutsch-Französisches Forschungsinstitut, ISL, St. Louis, France)

Fig. 6.4 Shadowgraph of a shock wave diffracting around a vertical wedge; vortex formation at the apex of the wedge (courtesy Deutsch-Französisches Forschungsinstitut, ISL, St. Louis, France)

An indirect determination of the density distribution in a flow was proposed for cases when a numerical solution of the flow field is available: by inserting the computed density distribution $\rho(x, y, z)$ into (6.2), one may construct a shadow pattern, and it is common to conclude that the numerical solution is correct if the computational and the experimental shadowgraphs look alike [6.7, 8]. Such procedures, that are taken as *validation* of the computational results, are also known for the methods described in the following sections. It appears that any conclusion about the validity of the numerical result from a similarity of the computed and experimentally visualised flow patterns must be done very carefully, because small deviations of the two patterns might still be associated with large differences in the respective density distributions.

The most drastic change in the second derivative of n or ρ occurs in a shock wave. The shadowgraph is most

appropriate for visualising the geometry of shock patterns, either a steady configuration in supersonic flow (Fig. 6.3), or unsteady configurations as produced in a shock tube (Fig. 6.4). Many shadow pictures of flows can be observed outside the laboratory. On a screen or wall one can easily see the shadow of a plume rising from a heat source, e.g. a candle, when the shadow is projected onto the wall by sunlight or light from a lamp. Another everyday experience is to observe the shadow pattern produced by a mixture of air and gasoline vapour when filling the tank of a car during sunshine. Sunlight also produces shadow pictures on the ground of a swimming pool due to the formation of waves on the free surface.

6.3 Schlieren Method

The German word *Schliere* designates an inhomogeneity or disturbance in a transparent medium, most often with reference to a glass plate or window. The credit for having introduced the schlieren method as a tool for visualising density inhomogeneities in a flow is usually given to Toepler, as outlined in the reviews of *Schardin* [6.9] and *Settles* [6.6], and the method is often referenced as the *Toepler schlieren method*, in order to distinguish this technique from other optical methods that are also associated with the word *schlieren* (see below). A system with parallel light through the test object, e.g. compressible flow, is considered (Fig. 6.5). An image of the light source is formed in the plane of the knife edge, which is placed in the focal plane of the second lens, called the *schlieren head*. Here, the knife edge is perpendicular to the plane of the figure, and the light source is either point-shaped or a narrow slit parallel to the knife edge. The camera lens serves to form an image of the test object on the recording plane (photographic film, chip of an electronic camera). Thus, the test object is in focus, and the formation of shadow effects (Sect. 6.1) is avoided.

If the light source is cutting off part of the image of the light source, the light intensity with which the recording plane is illuminated will be reduced. Let a be the reduced height of the light source image as seen in the direction of the optical axis (Fig. 6.6). An optical analysis [6.1, 6, 9] then delivers for the distribution of the relative light intensity in the recording plane

$$\frac{\Delta I}{I} = \frac{f_2}{a} \int_{\zeta_1}^{\zeta_2} \frac{1}{n} \frac{\partial n}{\partial y} \mathrm{d}z \,. \tag{6.3}$$

As in (6.1), $n(x, y, z)$ is the refractive index in the fluid flow, $I(x, y)$ is the light intensity in the recording plane, f_2 is the focal length of the schlieren head, and z is the direction of the optical axis. Note the integration of the information along the trajectories of the light in the test object, i. e. from ζ_1 to ζ_2. Equation (6.3) is derived under the assumption of very small angles of light deflection, ε (Fig. 6.1). If the system is applied to a gas flow, then $n \approx 1$, and with the Gladstone–Dale constant K, the equation can be written as

$$\frac{\Delta I}{I} = \frac{K f_2}{a} \int_{\zeta_1}^{\zeta_2} \frac{\partial \rho}{\partial y} \mathrm{d}z \tag{6.4}$$

from which it follows that the schlieren method is sensitive to changes of the density derivative normal to the knife edge, here $\partial\rho/\partial y$, because the knife edge in Fig. 6.5 is assumed to extend in the x-direction. By turning the knife edge (and the slit source) by 90° around the optical axis, one measures the component $\partial\rho/\partial x$.

From (6.3, 4) it follows that, for a given density distribution in the flow, the relative change in light intensity

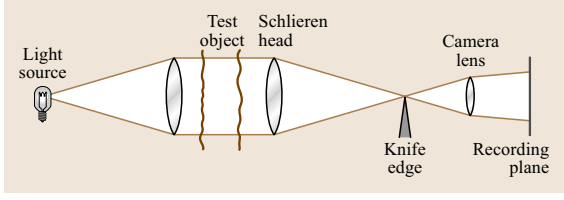

Fig. 6.5 Schlieren setup with parallel light through the test field

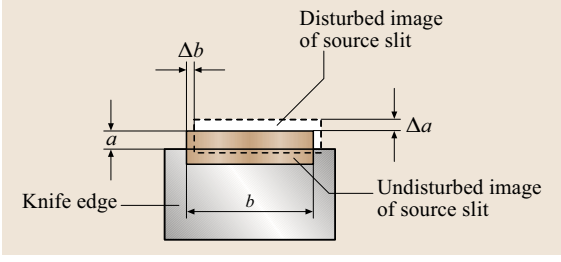

Fig. 6.6 Image of a light source of size $a \times b$ in the focal plane of the schlieren head, as seen in the direction of the optical axis; shift of the light source by Δa and Δb, respectively, caused by light deflection in the refractive index object

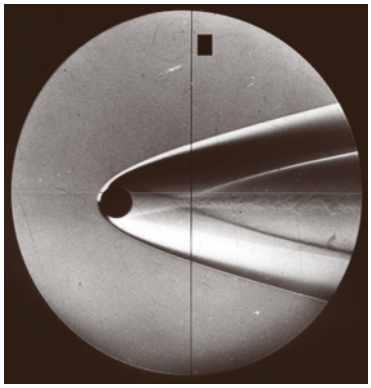

Fig. 6.7 Schlieren photograph of a sphere flying at supersonic velocity [6.1]

and therefore the contrast in the recording plane is larger the smaller the ratio a/f_2. Usually, in a schlieren setup it is not possible to replace the schlieren head during an experiment, and f_2 might be taken as fixed. There are several reasons why a cannot be reduced arbitrarily, the most important being diffraction, whose influence on the image quality must be avoided. Another reason results from the demand that the system should be capable of measuring light deflections in positive and negative directions, in Fig. 6.1 expressed by $+\varepsilon_y$ and $-\varepsilon_y$ when the knife edge is in the x-direction. In the schlieren system shown in Fig. 6.5 $+\varepsilon_y$ generates an increase of the light intensity, $-\varepsilon_y$ an intensity loss. Therefore, a should be chosen such that, in the undisturbed case, the (background) intensity of illumination is reduced, and light deflections in the positive and negative direction can be distinguished by a brighter or darker illumination at the respective position in the schlieren image (Fig. 6.7). High image quality is obtained if the background intensity in the recording plane, e.g. illumination without flow, is constant throughout this plane. This requires the use of a point source or slit source with minimal slit height a.

The term *schlieren method* is limited to optical systems in which the light distribution in the image of the source (focal point of schlieren head) is somehow manipulated, here by the knife edge. This should be kept in mind if the word *schlieren* appears in connection with other methods that are based on different optical principles (*background oriented schlieren* and *synthetic schlieren* in Sect. 6.4, and *schlieren interferometer* in Sect. 6.5). The *manipulation* of light can be defined more precisely, if one follows the descriptions of the schlieren method by means of system analysis or Fourier optics [6.10–12]. In terms of these analyses the knife edge acts, in the Fourier domain, as a frequency filter cutting off part of the transmitted frequency spectrum.

A great variety of modifications are reported in the literature; these aim at increasing the diameter of the light beam transmitted through the object, allowing the study of extended test objects, increasing the optical sensitivity towards the resolution of weak density changes, introducing some kind of quantitative assessment of the signal, etc. [6.1,6]. A closer look at the proposed modifications shows that almost none of these were not already included in Schardin's fundamental work on schlieren systems [6.9]. The most interesting extension of the classical schlieren system, whose signal pattern is a planar distribution of grey levels, is the addition of colour to the signal pattern, e.g. by means of a transparent colour filter that replaces the schlieren knife edge. In addition to the production of very decorative flow pictures, the use of

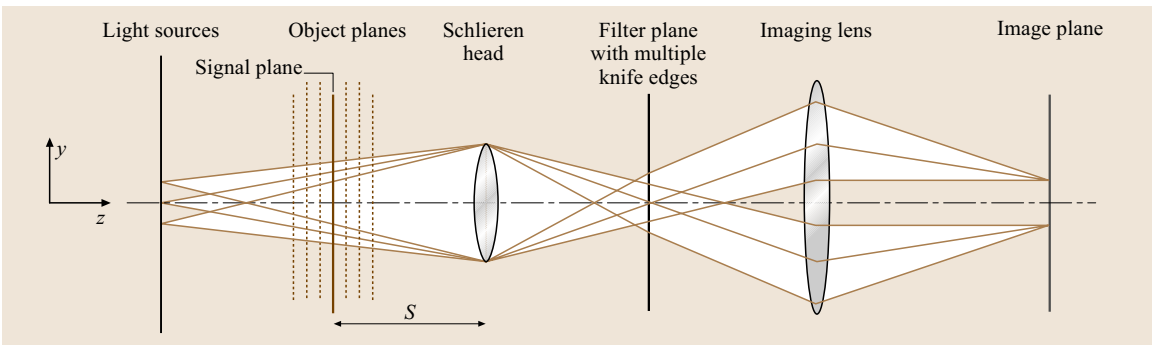

Fig. 6.8 Principle of a *sharp-focusing* schlieren system. Several light beams (*channels*, only three shown here), each originating from a source in the source plane, pass through the test field in different directions. Every channel has its knife edge in the filter plane where the schlieren head forms an image of each source. The signal plane at a distance S from the schlieren head is imaged onto the image plane. The 3-D refractive index field can be scanned by imaging different object planes onto the imaging plane

colours allows one to discriminate between the refractive deflection of light in the positive and negative directions, as well in the x- and y-directions; *Settles* [6.6, 13] presents the most complete and informative review of colour schlieren systems.

Due to the *line-of-sight* effect, in (6.2, 3, 4) expressed by the integration along z, information on $\partial\rho/\partial y$ or $\partial\rho/\partial x$ can be obtained directly only for a nominally two-dimensional (2-D) object with $\rho = \rho(x, y)$. Information on a three-dimensional (3-D) flow field is available by applying the techniques of optical tomography (Sect. 6.6). However, for the schlieren method, a special approach for resolving a 3-D density field is known. The *sharp-focusing schlieren system* [6.14] uses multiple off-axis point sources, with light beams or *channels* originating from each source and traversing the 3-D test field in different angular directions (Fig. 6.8). Each source has a corresponding knife edge or filter in the focal plane of the schlieren head. The image plane where all channels overlap is focused onto a particular plane in the object, normal to the z-direction, and the information from the overlapping signals is a measure of the desired quantity, here the fluid density gradient, in the focused object plane, while the contributions to the signal from regions outside of the focused object plane average out and reduce to noise. In practice, the focused object plane is a slice with small but finite extension in the z-direction, the direction of the optical axis. By means of the imaging lens, the position of the object plane, which is in focus, can be varied, and the 3-D object can thus be scanned in the z-direction.

Extensive information on the setting up of such a *sharp-focusing* or *multiple-source* schlieren system has been given by *Weinstein* [6.14]. Both from experiments and numerical simulations [6.12, 15] it is apparent that using five sources or channels provides a spatial resolution of the object that is barely improved by increasing this number. It cannot be expected that a satisfactory determination of the 3-D density distribution $\rho(x, y, z)$ is possible with this technique. However, it has been proven that valuable information on the spatial distribution of flow structures in compressible turbulent flows can be obtained with the *sharp-focusing* schlieren technique [6.16].

6.4 Moiré Deflectometry

Due to light deflection by a variable density field a geometrical pattern seen through this field appears deformed. The local deflections are described quantitatively by the displacements Δ_x and Δ_y shown in Fig. 6.1. Since these displacements are a measure of the respective deflection angles ε_x and ε_y, the measurement of the local displacement of the geometrical pattern, as seen in the recording plane, allows one to determine the local deflection angles and thus the derivatives of the density, $\partial\rho/\partial x$ and $\partial\rho/\partial y$, which are linked to the deflection angles by integral relationships similar to (6.4).

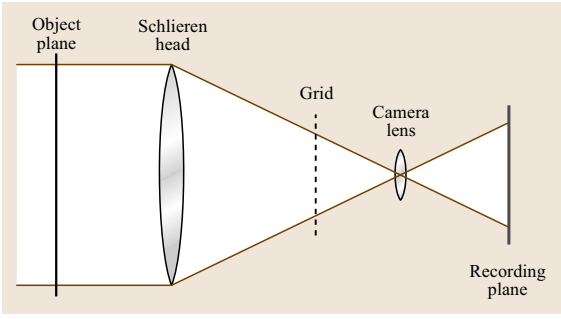

Fig. 6.9 Possible setup for deflection mapping by a Ronchi grid

The deformation of a given pattern when viewed through a density field is a phenomenon of daily experience; e.g. it can be realised if an object is observed through the warm air (plume) rising from a candle flame. The use of this effect for quantitative measurement has been known for a long time [6.1]. The geometrical pattern used for this purpose can be regular or random. When a regular pattern in the form of a grid is used, the technique is known as the *moiré method*; other names are *deflection mapping* or the *Ronchi method* (with a *Ronchi grid*). The grid, which can be placed on either side of the test object, can be different in shape, showing, e.g., equidistant lines, or regular patterns of concentric circles or squares. In principle, one observes through the test field a pattern of known geometry, which is distorted due to the refractive deflection of the light rays in the density field (Fig. 6.9). Many variations of moiré grids or patterns have been reported, including the use of two grids, one on either side of the test object, such that a situation that resembles the fringe patterns of an interferometer can be generated (Sect. 6.5).

These moiré or Ronchi methods are based on the use of a regular and macroscale geometrical reference pattern; *macroscale* in the sense that the grid dimensions are not very small in comparison to typical scales of

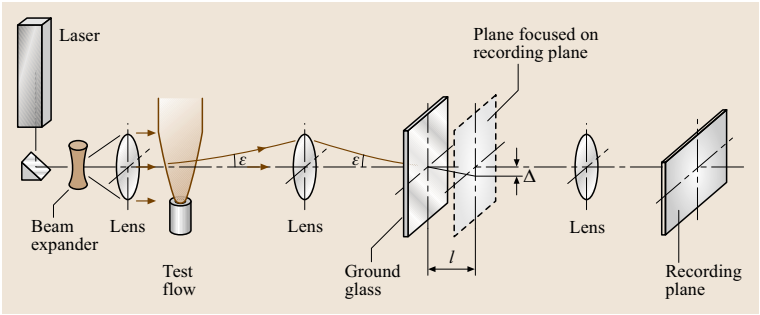

Fig. 6.10 Setup for deflection mapping by speckle photography [6.17]

the flow field to be visualised. In contrast to this situation, for the methods named *laser speckle photography*, microscale reference patterns of random geometry are used. These patterns, whose deformation caused by the refractive light deflection is studied, are generated by the optical speckle effect; for reviews see [6.17–19].

In the optical setup a ground glass placed in the light beam serves as the speckle-generating element (Fig. 6.10). Here, the test object is placed in front (left side) of the ground glass, and is imaged by means of a lens onto the plane of the ground glass, while the recording plane is focused onto a plane at a distance l from the ground glass. With a laser light source, optical speckles are generated to the right of the ground glass as a result of multiple interference of the light scattered from the elements of the ground glass. Two exposures are recorded and superimposed with the arrangement shown in Fig. 6.10: one exposure in the absence of the test object, and a second exposure with the object. Due to the refractive deflection in the second exposure, corresponding light rays from the two exposures appear separated by a displacement Δ in the plane at a distance l from the ground glass. The two components of this displacement, Δ_x and Δ_y, can be measured simultaneously in the recording plane, and with the relationship $\varepsilon \approx \Delta/l$, the two components of the density derivative, $\partial\rho/\partial x$ and $\partial\rho/\partial y$, can be determined. Since the speckle pattern as the reference pattern has a fine and evenly distributed structure, the distribution of $\boldsymbol{\Delta}(x, y)$ can be measured practically at any point in the recording plane, i. e. with very high spatial distribution, in contrast to the methods using regular (macroscale) grids, where the information is only available at the position of the grid lines.

The key for a successful application of the speckle method is the evaluation of the two recorded, superimposed speckle patterns by means of digital image processing. The same procedures as used for particle image velocimetry are used here, e.g., evaluation by means of correlation techniques, in order to determine the distribution of the displacement vectors $\boldsymbol{\Delta}(x, y)$ (Sect. 5.3.2). In fact, such evaluation algorithms on the basis of correlation schemes were developed for the speckle method prior to their use in particle image velocimetry. Speckle photography renders no direct visualisation of the flow with density variations; a visualisation is possible by subjecting the recorded speckle pattern to a spatial filtering process, and the result is similar to a schlieren pattern, but with much lower image quality [6.17–19].

While the speckle method uses a speckle pattern generated purposely by inserting a ground glass into the light path, the *background oriented schlieren method* makes use of a reference pattern that is naturally available, e.g., the structure of the background in the rear of the transparent object under study [6.20]. The background pattern as seen through the test region is recorded twice: once without flow, a second time with flow. The two overlapping patterns differ slightly due to the refractive deflection of the light in the test flow and, as in the case of the speckle method, the local displacement vectors $\boldsymbol{\Delta}(x, y)$, which are a measure of the light deflection angles $\varepsilon(x, y)$, can be determined by digital image processing (correlation methods). This technique has practically no limit regarding the diameter of the field of view, and allows the study of large test objects outside the laboratory. Here, the term *schlieren* is used because the method gives information on the deflection angle or the density derivative, like a schlieren system; but this term is misleading here because the setup is not a schlieren system according to the definition given in Sect. 6.3. The same argument applies to a method called *synthetic schlieren* which uses, in principle, two moiré grids [6.21]. However, in contrast to the scales applicable to conventional methods, the second grid is *virtual* and employs the digitisation of the field of view and the edges of pixels to form a reference pattern.

In contrast to *classical* schlieren technique (Sect. 6.3), all moiré methods aim to provide quanti-

tative information on the amount of light deflection in the flow with density variations. In comparison to schlieren, the optical setup is less sensitive to disturbances and therefore less costly, it is easier to investigate objects of large dimension, and the application of digital image processing for quantitative evaluation is straightforward; but the visual impression of schlieren pictures is probably much bigger; schlieren pictures, if well made, can appear more attractive than moiré records, and the optical sensitivity of the schlieren system is perhaps higher than that of a moiré setup.

6.5 Interferometry

The change in optical phase of a light wave transmitted through the flow field can be measured by instruments known as interferometers. The instruments applied to optical flow visualisation or the measurement of fluid density are exclusively *two-beam interferometers*, i. e., the visible signal pattern, called an *interferogram*, is the result of optical interference of two light waves, of which at least one is transmitted through the object. If this object wave interferes with a second wave that remains undisturbed and thus serves as a reference, one has *reference beam interferometry*. If both waves pass through the object field, but displaced by a small distance with respect to each other or *sheared*, they belong to the class of *shearing interferometry*, sometimes also called *differential* or even (and without technical reason) *schlieren interferometry*.

The principle of two-beam interferometry is explained in Fig. 6.11 by considering light rays instead of waves [6.1]. A parallel beam of light is passed through the test object along the z-direction. Each ray of the beam is considered to interfere with a conjugate ray separated from the first ray by a distance d. Fig. 6.11 is a projection of the y–z plane; the test field is bounded by the surfaces $\zeta_1(x, y)$ and $\zeta_2(x, y)$, and for the following analysis it is assumed that these surfaces are planes $z = \text{const.}$, which is no general restriction. Behind the test object, a lens or mirror, equivalent to the *schlieren head* in Sect. 6.3, focuses the light beam, and a black box, here called the *interferometer unit*, ensures that all *conjugate rays* either coincide after having passed through this unit, or are made to intersect in the recording plane, where they interfere and produce the visible interference pattern.

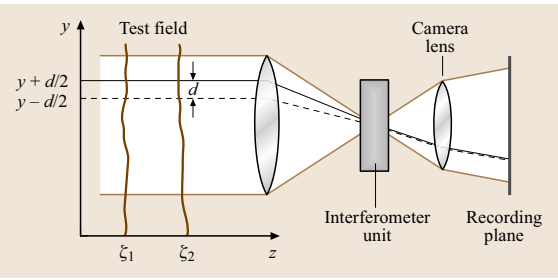

Fig. 6.11 Principle of a two-beam interferometer with parallel light through the test field

The difference in optical path length between two conjugate rays is

$$\Delta l = \int_{\zeta_1}^{\zeta_2} n\left(x, y+\frac{d}{2}, z\right) \mathrm{d}z - \int_{\zeta_1}^{\zeta_2} n\left(x, y-\frac{d}{2}, z\right) \mathrm{d}z \,. \tag{6.5}$$

The optical phase difference is obtained by dividing Δl by the wavelength λ. Bright interference fringes appear in the recording plane where

$$\frac{\Delta l(x, y)}{\lambda} = 0, \pm 1, \pm 2, \ldots \,, \tag{6.6}$$

which therefore represents the equation of fringes in the recording plane (the integers designate the *fringe order*). Thus, $\Delta l(x, y)/\lambda$ is the signal in planar form, which serves to determine the unknown quantity n; the problem that the signal is two dimensional, whereas the quantity of interest $n(x, y, z)$ is three dimensional, was mentioned above (*line-of-sight* methods). However, (6.5) incorporates a further problem: three is only one equation for two unknowns, namely n at two different positions, $y + d/2$ and $y - d/2$. A solution to this problem is provided by an appropriated design of the *interferometer unit* in Fig. 6.11, thereby reducing the number of unknowns to only one. Two different approaches that define two different classes of interferometers are known. They are characterised by the magnitude of the ratio d/D, with D being the diameter of the field of view or the diameter of the parallel light beam in Fig. 6.11:

1. With $d/D \geq 1$, one ray of each pair of conjugate rays propagates outside the test field, where it remains undisturbed; this is the class of *reference beam interferometers*. One of the two integrals in (6.5) that

describes the optical path covered by the *reference beam* reduces to a constant.

2. For $d/D \ll 1$, both rays traverse the test field, where they are separated or *sheared* by the small distance d. It is common to call such systems *shearing interferometers*. Developing (6.6) into a Taylor series around the value of $n(x, y, z)$ and taking into account only the linear terms (the quadratic terms vanish), because d is a small quantity, results in

$$\frac{d}{\lambda}\int_{\zeta_1}^{\zeta_2}\frac{\partial}{\partial y}n(x, y, z)\,\mathrm{d}z = 0, \pm 1, \pm 2, \ldots \qquad (6.7)$$

as the equation of fringes for a shearing interferometer. It is seen that the signal is proportional to the first derivative of the refractive index or the gas density, as is the case for schlieren systems (6.3, 4), which explains the name *schlieren interferometer*, occasionally used for this class of instruments. Another name, *differential interferometer*, results from the appearance of the derivative in (6.6). The derivative $\partial n/\partial x$ can be measured by rotating the system around the optical axis (z-axis) by 90°.

Equations 6.6 and 6.7 apply to alignment of the interferometer for which a uniform test field (with $n = \text{const.}$ or $\partial n/\partial y = \text{const.}$) appears uniformly illuminated, i. e., no fringes are seen in the field of view. This case is called the *infinite fringe width* (IFW) alignment. Both interferometers can be aligned in a different way, so that a system of equidistant, parallel interference fringes appears for the uniform test field. A density variation in the flow will distort this regular fringe pattern, and the deviation or shift of a fringe from its undisturbed position is then the signal and a measure for the density variation. An alignment with this signal form is called the *finite fringe width* (FFW) alignment. A fringe shift by one fringe width (a distance S of the fringes in the undisturbed case) is equivalent to a difference in optical path length of one wavelength. It follows that a fringe shift ΔS at a point (x, y) measured in terms of the width S is

$$\frac{\Delta S(x, y)}{S} = \frac{1}{\lambda}\int_{\zeta_1}^{\zeta_2} n(x, y, z)\,\mathrm{d}z - \text{const.} \qquad (6.8)$$

for the reference interferometer, and

$$\frac{\Delta S(x, y)}{S} = \frac{d}{\lambda}\int_{\zeta_1}^{\zeta_2}\frac{\partial}{\partial y}n(x, y, z)\,\mathrm{d}z \qquad (6.9)$$

for the shearing interferometer. The experimenter can select either the IFW or FFW alignment; the choice is made according to the special experimental conditions.

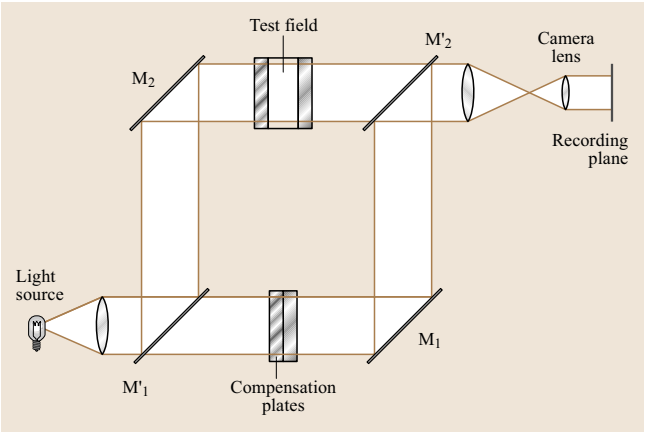

Fig. 6.12 Principal setup of a Mach–Zehnder interferometer; M_1, M_2 are mirrors; M'_1, M'_2 are beam splitters

The classic reference beam instrument is the Mach–Zehnder interferometer (MZI), which has been in use since the end of the 19th century. It is designed to allow a wide separation of test and reference beam, i. e., $d/D > 1$ (Fig. 6.12). The *interferometer unit*, mentioned in Fig. 6.11, is here the second beam splitter M'_2, while the first beam splitter M'_1 separates the incident beam into the test and reference beam. If all mirrors and beam splitters, M_1, M_2, M'_1, M'_2, are aligned exactly parallel, one has the IFW mode. Tilting one of the plates, usually M'_2, provides the FFW mode. For flow studies, particularly in a wind tunnel, a large-diameter field of view D is desired. This results in tight requirements on the optical and mechanical precision of the mirrors, beam splitters, test section windows, and compensation plates (which compensate for the optical path length experienced by the test beam in the test section windows). These requirements made the MZI a very expensive instrument, difficult to handle, and sensitive to mechanical disturbances or vibrations. The invention of holography opened a new route to develop an attractive alternative to the MZI: holographic interferometry.

The key to holographic interferometry is that it is possible to store on one holographic plate the information of two (or more) light waves and to simultaneously release, or reconstruct, the originally separate information in each [6.5, 22]. The reconstructed waves coincide spatially and can interfere if the conditions for optical coherence are fulfilled. In a holographic interferometer two consecutive holographic exposures are taken through the field of interest, most often the first exposure without flow, and the second in the presence of the flow with varying fluid density. Here, the first

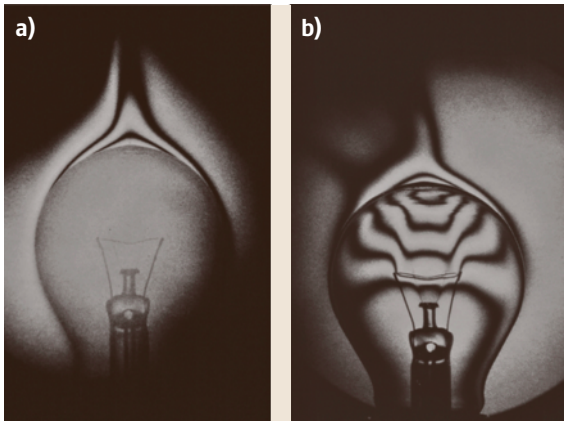

Fig. 6.13 **(a)** Mach–Zehnder interferogram visualising the plume rising from a hot light bulb (IFW mode). **(b)** Holographic interferogram visualising the temperature fields outside and inside the hot bulb (IFW mode)

exposure is the reference wave, while the second exposure carries information about the flow and is therefore the test wave. Upon simultaneous reconstruction of the two holographic recordings, one produces an interfering wave pattern equivalent to the interfering test and reference beams in the MZI. The difference between the two approaches is that in the MZI the reference and test beams exist simultaneously but are separated in space, whereas in a holographic interferometer the two beams coincide spatially but are separated in time, because they are recorded at different instants of time. From this spatial coincidence follows an important advantage of holographic interferometry compared to Mach–Zehnder interferometry: disturbances in the optical components of the setup, which cause distortions of the MZI fringe system, are cancelled out in a holographic interferometer because they affect the test and reference beam in the same way and at the same position. This is exemplified in Fig. 6.13. The Mach–Zehnder interferogram of a hot light bulb visualises the plume rising in the air above the bulb, but nothing is seen inside the bulb because the glass is low quality, and thus does not allow interference of light rays that pass through the bulb. In the holographic interferogram the disturbances caused by the bulb glass are compensated, and interference fringes visualise the temperature field inside the bulb.

In a typical setup of a holographic interferometer (Fig. 6.14) a laser beam is separated by a beam splitter into two beams. One of them, after being expanded, traverses the test field as a collimated beam and then strikes the holographic plate in the recording plane. The second beam is fed outside the test field where it remains undisturbed and, after expansion by a second beam expander, it also strikes the holographic plate. This second beam is needed as the holographic reference beam, and its role must not be confused with that of the reference beam in the MZI. The holographic reference beam is also needed to reconstruct the object from the hologram [6.22].

A number of modifications of the holographic setup shown in Fig. 6.14 are described in the literature, among which some allow the recording of real-time holographic recordings by means of cinematography. A particular modification of the setup is the generation of a certain degree of three-dimensional information. For this purpose it is necessary to introduce a ground glass as a light diffuser into the optical path, designated by D in Fig. 6.14. The diffuser scatters the light into various directions, such that a continuum of beam directions traverses the test field and, as a consequence, the reconstructed scene may be examined under different viewing angles. In this way, different interferograms can be produced from the same holographic exposure for each viewing angle. However, the total angle of possible viewing directions is limited, and one holographic interferogram of this

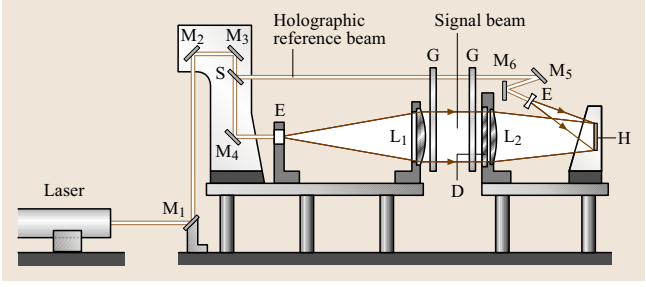

Fig. 6.14 Setup of a holographic interferometer [6.1]. M_1–M_6 mirrors; L_1, L_2 lenses; S beam splitter; E beam expander; G glass windows of test section; D diffuser (ground glass); H holographic plate

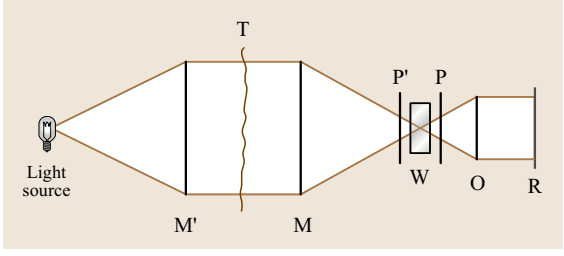

Fig. 6.15 Setup of a shearing interferometer using a Wollaston prism W and parallel light through the test field T; M, M′ are lenses or spherical mirrors; P, P′ polarisers; O imaging lens; R recording plane

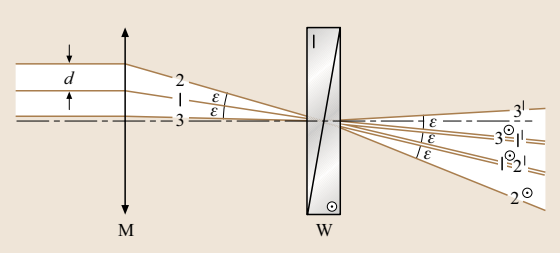

Fig. 6.16 Shearing of the light beam by the Wollaston prism W; M is the schlieren head (Fig. 6.15)

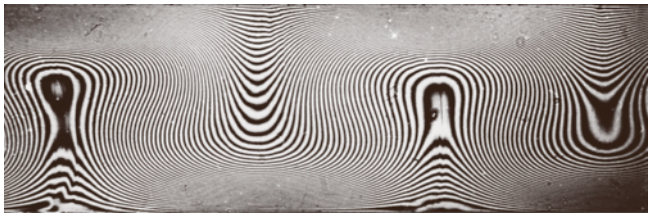

Fig. 6.17 Mach–Zehnder interferogram of Bénard convection in a 2-D liquid fluid cell; fringes are curves of constant temperature (W. Merzkirch)

kind is usually not sufficient for a complete tomographic study of the test field; see Sect. 6.6.

The dependence of a shearing interferometer's signal on the (first) derivative of the density (6.7, 9) makes these devices interesting for studies in convective heat transfer. A great variety of shearing interferometers are known; the most common setup applied in flow studies uses a Wollaston prism as the *interferometer unit* [6.1]. The setup sketched in Fig. 6.15 is similar to that of a schlieren system; the knife edge is simply replaced by the combination of the Wollaston prism with two polarisers, one in front and one behind the prism, and the two polarisers rotated by 90° with respect to each other. The similarity with the schlieren system is another reason for the name *schlieren interferometer*. A Wollaston prism splits each incident ray into two diverging rays separated by an angle ε, which is given as a constant of the system (Fig. 6.16). The two separated rays are linearly polarised, with polarisation directions normal to each other, in Fig. 6.16 characterised by the symbols $\otimes$ and |. It can be seen that each ray $i\otimes$ coincides with a ray $(i+1)|$, and these two rays (or waves) can interfere due to the presence of the second polariser behind the prism. The first polariser in front of the prism (Fig. 6.15) simply provides equal intensity of the conjugate rays. The two interfering rays traverse the test field at different positions, separated by the distance d (Fig. 6.16). The quantity d is the product of the focal length of the lens (or *schlieren head*) M and the separation angle ε (with $\varepsilon \ll 1$).

If the centre of the prism coincides with the focal point of M (Fig. 6.15), and if there is a homogeneous density distribution in the test field, all interfering rays will not exhibit a phase difference, and the field of view is free of interference fringes (*infinite fringe width* alignment, IFW). A shift of the prism from this central position along the optical axis (z-direction) results in the formation of parallel, equidistant fringes (*finite fringe width* alignment, FFW). It can be shown [6.1] that the fringe width in the FFW mode is

$$S = \frac{\lambda f_2}{\varepsilon w} \tag{6.10}$$

with λ being the wavelength of the used light source, f_2 the focal length of M, ε the separation angle of the Wollaston prism, and w the shift of the prism from the central position along the optical axis. The direction of the measured density gradient [y in (6.9)] is normal to the undisturbed fringes in the FFW mode. A vertical shift of the prism causes no change in the fringe width; it only changes the order of the fringes appearing in the field of view [6.1].

In a shearing interferogram solid contour lines, e.g. the edge of a solid body or the frame of the field of view, appear in the form of a double image or gray band of width $d\cos\alpha$, where α is the angle between the direction of shear [y in (6.9)] and the normal to the wall. The exact position of the wall edge is in the middle of the gray band. A shock wave causing a density jump is also depicted as a band of width $d\cos\alpha$.

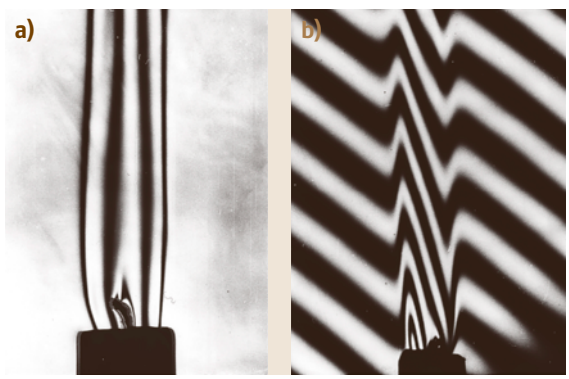

Fig. 6.18a,b Plume rising from a candle flame visualised by a Wollaston prism shearing interferometer; **(a)** IFW mode; note the double image of the candle contour line; **(b)** FFW mode (W. Merzkirch)

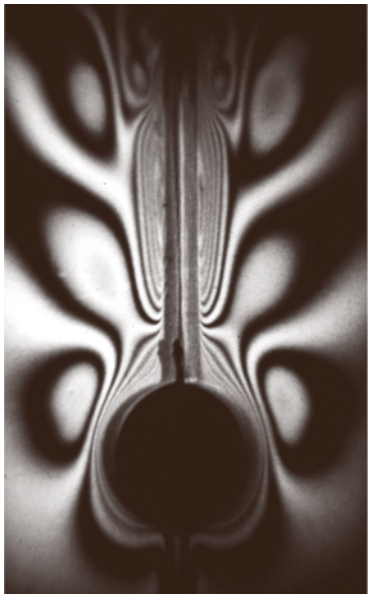

Fig. 6.19 Formation of an internal gravity wave in density-stratified saltwater visualised by a shearing interferometer; near field around a solid cylinder towed in the downward direction (W. Merzkirch)

Typical examples of interferograms are presented in Figs. 6.17, 6.18, 6.19. They include a reference beam interferogram of a two-dimensional flow field taken in the IFW mode such that the fringes are curves of constant density (here constant temperature), and shearing interferograms in the IFW and FFW modes, one taken with a *white* light source and therefore being coloured since the position of the fringes then depends on the wavelength λ (6.7).

In an interferogram the information on optical path length or optical phase, and therefore on fluid density, is given along the interference fringes. As expressed by (6.5) and (6.7) this information is available in discontinuous form, because the fringes are separated by a path length difference of a wavelength or by a phase difference of 2π. A number of methods have been communicated for automated evaluation of an interferogram, and have been continuously improved along with the progress made in digital image processing (e.g. [6.24]). With these methods it is possible to interpolate the information in the space between two interference fringes. The result of such an interpolation is less precise, the lower the number of fringes in the field of view, which means that the measurement accuracy will be low for weakly refractive test objects.

A nearly continuously distributed measurement of optical phase or optical path length in the recording plane is possible with *digital phase-stepping interferometry*, a combination of holographic interferometry and computer-based signal evaluation [6.23]. Here, the interferogram's phase is manipulated in a known manner such that it can be displayed as a gray scale and determined very accurately at a large number of points in the image plane. During the reconstruction process the holographic reference beam (Fig. 6.14) is translated step by step, with each step being a fraction of a wavelength. In this way, the constant appearing in (6.5), when this equation applies to a reference beam interferometer, is altered within fractions of a wavelength, or the constant optical phase of the interferometric reference beam is altered, step by step, by fractions of 2π. These stepwise alterations result in changes of the image intensity, which can be recorded by a digital camera and calibrated for further evaluation in the form of a look-up table [6.25]. Quantitative optical information in the space between two *regular* interference fringes is now available as the result of a physical process and not only by numerical interpolation and, hence, the sensitivity of interferometric methods for weakly refractive objects is increased by at least one order of magnitude (Fig. 6.20). While the resolution of a conventional interferometer is usually given as 1/10 of a wavelength (this value must be converted into values of density with the equations given above and with application to a particular object), the resolution of digital phase stepping is estimated to be between 1/100 and 1/1000 of a wavelength [6.23].

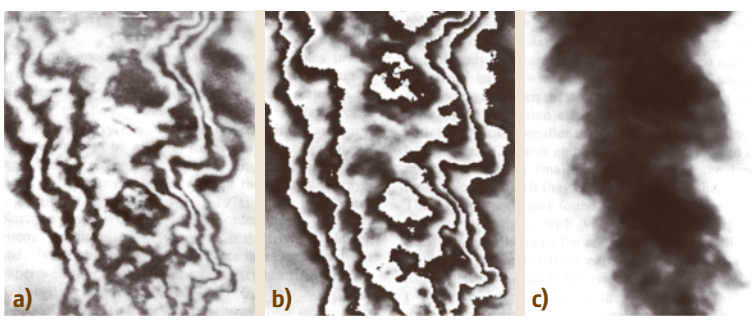

Fig. 6.20 **(a)** Reference beam interferogram of a transitional helium jet; **(b)** phase display in the form of a digital interferogram; **(c)** gray scale display of absolute phase of **(a)** (courtesy Prof. D. W. Watt, University of New Hampshire, USA [6.23])

6.6 Optical Tomography

As noted in Sect. 6.1 line-of-sight methods integrate the optical information on the density distribution in the object field along the light path in the fluid. Techniques for desintegrating the signal pattern and providing local data values of the 3-D density (or density gradient, respectively) are called optical tomography. These techniques are based on the possible transformation of the z–y Cartesian coordinate system (the x coordinate is not considered here for simplicity) into a z–α coordinate system, with α being the angle of the direction under which a point z, y is seen from the origin (0, 0). If one restricts the field of interest to values $z \geq 0$, then all values α cover a range of 180°. The idea is that the light beam of the optical system is directed through the object field in multiple directions α (*projections*) in order to *reconstruct* the density function $\rho(z, y)$ from the multiple of signal patterns obtained for each transmission direction α. That this is possible becomes evident from Fig. 6.21, where the object field is discretised into a finite number of elements, each including a constant value of the density (or gradient, respectively) $\rho_i (i = 1 \ldots N)$; the values ρ_i are the unknowns that must be determined from a set of N equations. With the discretisation the integral, e.g. in (6.5), is replaced by a summation; each projection provides a number of equations $n < N$ that link the signal pattern recorded for the projection α_j with n unknowns. The projections in different directions α_j serve to produce a sufficient number (N) of independent equations.

A number of algorithms for optical tomography have been described in the literature; see, particularly [6.26]. The aim of most approaches is to provide high 3-D resolution of the reconstruction with a minimum number of projections. In analogy to the formerly mentioned z–α coordinate system, a total angular range of projections of 180° is needed to reconstruct a random 3-D object field. Any symmetry in the object reduces the number of necessary projections and, possibly, the total angular range to be covered. The simplest case is an axisymmetric object, which can be reconstructed with only one projection using the Abel inversion as the reconstruction algorithm [6.1].

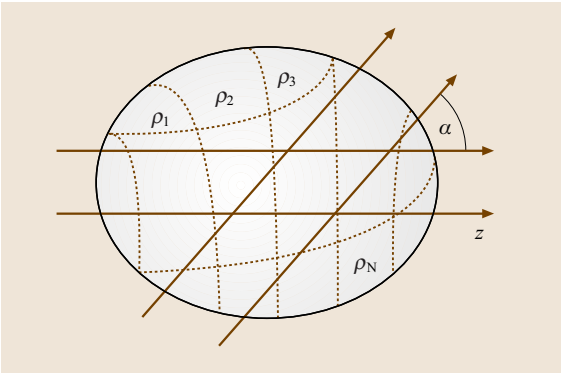

Fig. 6.21 Discretisation of the refractive index field into N elements with constant value of the density ρ_i; variation of projections for optical tomography

The majority of tomographic methods apply to optical interferometry, e.g. [6.27, 28]. A complex and elaborate optical setup is needed for the investigation of unsteady flows because the interferograms of all projections must be recorded simultaneously [6.29]. An accurate 3-D reconstruction requires a dense distribution of the signal in the recording planes. Since the signal density in an interferogram is limited, attempts have been made to use the high data rate available with optical speckle densitometry (Sect. 6.4) for more-precise tomographic reconstructions of flows with varying fluid density [6.30]. Finally, it should be noted that tomography can provide the spatial resolution necessary for evidencing turbulent large-scale structures, but not yet, at this state of the development, for resolving turbulent fine scales.

References

6.1 W. Merzkirch: *Flow Visualization*, 2nd edn. (Academic, Orlando 1987)

6.2 F. Peters: A compact presentation of gasdynamic fundamentals, Forsch. Ingenieurw. **68**, 111–119 (2003)

6.3 F.J. Weinberg: *Optics of Flames* (Butterworth, London 1963)

6.4 W. Lauterborn, A. Vogel: Modern optical techniques in fluid mechanics, Annu. Rev. Fluid Mech. **16**, 223–244 (1984)

6.5 F. Mayinger, O. Feldmann (Eds.): *Optical Measurements*, 2nd edn. (Springer, Berlin, Heidelberg 2001)

6.6 G.S. Settles: *Schlieren and Shadowgraph Techniques* (Springer, Berlin, Heidelberg 2001)

6.7 W. Schöpf: A new way of analyzing the shadowgraph method, J. Flow Vis. Image Proc. **4**, 179–187 (1997)

6.8 G.B. Brassington, J.C. Patterson, M. Lee: A new algorithm for analyzing shadowgraph images, J. Flow Vis. Image Proc. **9**, 25–51 (2002)

6.9 H. Schardin: Die Schlierenverfahren und ihre Anwendungen, Ergeb. Exakten Naturwiss. **20**, 303–439 (1942), in German

6.10 H. Wolter: Schlieren, Phasenkontrast und Lichtschnittverfahren. In: *Handbuch der Physik*, Vol. 24, ed. by S. Flügge (Springer, Berlin, Heidelberg 1956) pp. 555–645

6.11 C.A. Lopez: Numerical simulation of a schlieren system from the Fourier optics perspective, AIAA Paper **94-2618** (1994)

6.12 A. Hanenkamp, W. Merzkirch: Investigation of the properties of a sharp-focusing schlieren system by means of Fourier analysis, Opt. Lasers Eng. **44**, 159–169 (2006)

6.13 G.S. Settles: Colour-coding schlieren techniques for the optical study of heat and fluid flow, Int. J. Heat Fluid Flow **6**, 3–15 (1985)

6.14 L.M. Weinstein: Large-field high-brightness focusing schlieren system, AIAA J. **31**, 1250–1255 (1993)

6.15 S.H. Collicott, T.R. Salyer: Noise-reduction properties of a multiple-source schlieren system, AIAA J. **32**, 1683–1688 (1994)

6.16 S. Garg, G.S. Settles: Measurements of a supersonic turbulent boundary layer by focusing schlieren deflectometry, Exp. Fluids **25**, 254–264 (1998)

6.17 W. Merzkirch: Density-sensitive whole-field flow measurement by optical speckle photography, Exp. Thermal Fluid Sci. **10**, 435–443 (1995)

6.18 K.D. Kihm: Laser speckle photography technique applied for heat and mass transfer problems, Adv. Heat Transf. **30**, 255–311 (1997)

6.19 N.A. Fomin: *Speckle Photography for Fluid Mechanics Measurements* (Springer, Berlin, Heidelberg 1998)

6.20 M. Raffel, H. Richard, G.E.A. Meier: On the applicability of background oriented optical tomography for large scale aerodynamic investigations, Exp. Fluids **28**, 477–481 (2000)

6.21 S.B. Dalziel, G.O. Hughes, B.R. Sutherland: Whole-field density measurements by "synthetic" schlieren, Exp. Fluids **28**, 322–235 (2000)

6.22 C.M. Vest: *Holographic Interferometry* (Wiley, New York 1979)

6.23 D.W. Watt, C.M. Vest: Digital interferometry for flow visualization, Exp. Fluids **5**, 401–406 (1987)

6.24 H.H. Bartels-Lehnhoff, P.H. Baumann, B. Bretthauer, G.E.A. Meier: Computer-aided evaluation of interferograms, Exp. Fluids **16**, 46–53 (1993)

6.25 T.A.W.M. Lanen, C. Nebbeling, J.L. van Ingen: Digital phase-stepping holographic interferometry in measuring 2-D density fields, Exp. Fluids **9**, 231–235 (1990)

6.26 G.T. Herman: *Image Reconstruction from Projections* (Academic, New York 1980)

6.27 H. Philipp, T. Neger, H. Jäger, J. Woisetschläger: Optical tomography of phase objects by holographic interferometry, Measurement **10**, 170–181 (1992)

6.28 K. Muralidhar: Temperature field measurement in buoyancy-driven flows using interferometric tomography, Annu. Rev. Heat Transf. **12**, 265–375 (2002)

6.29 B. Timmerman, D.W. Watt: Tomographic high-speed digital holographic interferometry, Meas. Sci. Technol. **6**, 1270–1277 (1995)

6.30 T.C. Liu, W. Merzkirch, K. Oberste-Lehn: Optical tomography applied to speckle photographic measurement of asymmetric flows with variable density, Exp. Fluids **7**, 157–163 (1989)